ARTICLES SCIENCE CHINA Materials

mater.scichina.com link.springer.com

Published online 7 November 2019 | https://doi.org/10.1007/s40843-019-1195-7

Sci China Mater 2020, 63(3): 444–452

Size-dependent mechanical properties and deformation mechanisms in Cu/NbMoTaW nanolaminates

Yufang Zhao, Jinyu Zhang*, Yaqiang Wang, Kai Wu, Gang Liu* and Jun Sun*

ABSTRACT **High entropy alloys (HEAs) have attracted extensive attention due to their excellent properties in harsh environments. Here, we introduced the HEA NbMoTaW into the laminated structure to synthesize the Cu/HEA nanolaminates (NLs) with equal layer thickness *h* spanning from 5 to 100 nm, and comparatively investigated the size dependent mechanical properties and plastic deformation. The experimental results demonstrated that the hardness of Cu/HEA NLs increased with decreasing *h*, and reached a plateau at $h \leq 50$ nm, while the strain rate sensitivity *m* unexpectedly went through a maximum with reducing *h*. The emergence of maximum *m* results from a transition from the synergetic effect of crystalline constituents to the competitive effect between crystalline Cu and amorphous-like NbMoTaW. Microstructural examinations revealed that shear banding caused by the incoherent Cu/HEA interfaces occurred under severe deformation, and the soft Cu layers dominated plastic deformation of Cu/HEA NLs with large *h*.**

Keywords: high-entropy alloys, nanolaminated structure, interfaces, strain rate sensitivity

INTRODUCTION

High-entropy alloys (HEAs) break the traditional principle for alloy design and open a new area for exploring advanced materials [1–4]. The core effects of HEAs, including high-entropy effects, sluggish diffusion, severe lattice distortion and cocktail effects, enable coarse-grained (CG) HEAs to possess excellent mechanical properties, e.g., superior strength [5,6], high ductility [7–9], great thermal stability [10], excellent diffusion resistance [11] and good fatigue resistance [12,13]. For example, the hardness and compressive yield strength of the as-cast body-centered-cubic (BCC) TaNbHfZr [14] are 2.4 and 4.9 times of those expected from the rule-of-mixture (ROM), respectively. However, as the grain size (d) is reduced into submicron- and nano-scales, HEAs exhibit increased strength but greatly reduced tensile ductility [15,16] or deformability [17], similar to the cases of nanocrystalline (NC) pure metals [18,19]. Therefore, how to enhance the plasticity of NC HEAs, such as BCC NbMoTaW, with a minor (or without) loss of strength is very important for their applications in harsh environments, such as elevated temperatures, high rates of impact and radiation.

In fact, integrating the soft/ductile phase (e.g., Cu) and the hard/brittle phase (e.g., HEAs) to form nanolaminates (NLs) is an available strategy to suppress the nucleation/propagation of microcracks initiated in the hard/brittle phase, thus achieving great plasticity of the NLs [20–23]. It has been unambiguously demonstrated that it is the density of interfaces or the intrinsic layer thickness h that determines the unique mechanical properties of NLs. Previous studies [24] about conventional crystalline/crystalline NLs (C/CNLs), e.g., Cu/Cr [20], Cu/Ni [25] and Cu/Zr [22], and crystalline/amorphous NLs (C/ANLs), e.g., Cu/Cu-Zr [26], Cu/Pd-Si [27] and Cu/Cu-Nb [28], have uncovered the well-known size h-dependent strength (σ), i.e., "smaller is stronger", often for $h >$ ~5 nm. Moreover, three regimes of size-h dependent strength are divided based on the transition of strengthening mechanisms. (i) The dislocations pile-up mechanism when $h \geq 50$ nm. In this regime, dislocations generated in the soft layers move to the interfaces and are stopped by them to form a pile-up. (ii) The confined layer slip (CLS) mechanism when $10 < h < 50$ nm. In this regime, the hairpin dislocation is confined in the individual layer, since the interface barrier to dislocation transmission is

State Key Laboratory for Mechanical Behavior of Materials, Xi'an Jiaotong University, Xi'an 710049, China

*Corresponding authors (emails: jinyuzhang1002@mail.xjtu.edu.cn (Zhang J); lgsammer@mail.xjtu.edu.cn (Liu G); junsun@mail.xjtu.edu.cn (Sun J))

© Science China Press and Springer-Verlag GmbH Germany, part of Springer Nature 2019

higher than the gliding resistance. (iii) The dislocation cutting across the interface mechanism when $h \leq 10$ nm. In this regime, dislocations can generate from the interface or transmit across the interface because the interface barrier strength (IBS) is overwhelmed by the stress needed for CLS of hairpin dislocations.

In parallel, some experiments were carried out to study the size h-dependent strain rate sensitivity (SRS, m) of C/CNLs [29] as well as C/ANLs [30]. Although the structure of constituents (e.g., face-centered cubic (FCC), BCC and hexagonal-close-packed (HCP) metals) can influence their size-dependent SRS [22,31–33], the studies by Zhang *et al.* [22,34] have verified that Cu/Cr, Cu/Mo and Cu/Zr C/CNLs with incoherent crystalline/crystalline interfaces (CCIs) displayed monotonically increased m with decreasing h. Interestingly, when $h > 10$ nm, the m of highly textured Cu/Ni NLs increases with decreasing h, but the opposite holds when $h < 10$ nm due to the formation of coherent CCIs [29]. These results imply that the interfacial structure determines the rate-dependent mechanical responses of C/CNLs. Although limited studies about m of HEAs, such as BCC NbMoTaW [35] have shown that this NC HEA thin film behave the same way as their NC constituent siblings (e.g., BCC Mo and Ta), the rate-limiting process of HEAs in NLs under strong constraining conditions is still far from understanding. Specifically, the nanolaminated structure provides an ideal vehicle to investigate the size-dependent plasticity of HEAs in the deep nanoscale with the characteristic size < 50 nm.

In principle, the nanolaminated concept can be applied to any two-phase, bimetallic system; however, for a number of reasons, these C/CNLs have been limited to combinations of pure metals before. Motivated by above issues, here we introduce the HEA (HEA = NbMoTaW) into the nanolaminated structure, since the HEA bears several desirable intrinsic properties as mentioned above. We systematically study the size-dependent deformation behavior and mechanical properties of the equal layered Cu/HEA C/CNLs to comprehensively understand the underlying mechanisms of their fundamentally different mechanical behaviors.

EXPERIMENTAL SECTION

Materials preparation

The Cu/HEA (HEA = NbMoTaW) NLs with equal individual layer thickness (h) ranging from 5 to 100 nm were deposited on HF-etched (111)-Si wafers by direct current (DC) magnetron sputtering at room temperature. Pure Cu (99.995%) and NbMoTaW (99.95%) targets were used to prepare Cu/HEA NLs with the total thickness of ~1.5 μm. The sputtering chamber was evacuated to a base pressure of less than 4×10^{-4} Pa before deposition. The deposition rates for Cu and NbMoTaW were about 0.12 and 0.065 nm s^{-1}, respectively. The substrate was neither heated nor cooled during the deposition process. The first layer on the substrate was Cu and the cap layer was HEA. For the comparison purpose, ~1.5 μm-thick Cu and NbMoTaW monolithic thin films were also prepared under the same conditions.

Microstructure characterization

X-ray diffraction (XRD) experiments were carried out using a Bruker D8 Discover powder X-ray diffractometer with Cu Kα radiation at room temperature to determine the phase structure and crystallographic orientations of the NLs. Transmission electron microscopy (TEM) was performed on a JEOL JEM-2100F electron microscope equipped with energy dispersive spectroscopy (EDS) at the 200 kV accelerating voltage, to characterize the internal features of Cu/HEA NLs. To investigate the microstructural evolution during plastic deformation, post-mortem TEM observations were also performed on the indented Cu/HEA NLs. The TEM foils were prepared using a FEI Helios NanoLab 600i dual-beam focus ion beam (FIB) system *via* the lift-out technique.

Nanoindentation tests

Nanoindentation hardness (H) tests were conducted on all film materials using a TI950 TriboIndenter (Hysitron, Minneapolis, MN) equipped with a standard Berkovich diamond indenter with a nominal tip radius of curvature of 50 nm under the load-controlled mode at room temperature. Since the hardness reaches a plateau at an indentation depth 10%–15% of the total layer thickness, the maximum load (5500 μN) was chosen within a maximum indenting depth falling in this range to eliminate the substrate effects. The loading time varied from 5 to 100 s, corresponding to the strain rate ($\dot{\varepsilon}$) spanning from 0.005 to 0.1 s^{-1}, in order to obtain the SRS index m. The SRS is experimentally defined as the slope of the double logarithmic plot of hardness H and $\dot{\varepsilon}$ under isothermal conditions, which can be expressed as $m = \frac{\partial \log(H)}{\partial \log(\dot{\varepsilon})}$. The allowed drift rate was set as 0.01 nm s^{-1}, which is 10 times smaller than the typical value (0.1 nm s^{-1}) to guarantee the reliability and accuracy of the measurements. A minimum of 9 indents separated from each other of ~30

 © Science China Press and Springer-Verlag GmbH Germany, part of Springer Nature 2019

μm were performed on each sample at each strain rate to obtain the average hardness and standard deviation.

RESULTS

Initial microstructure of the as-deposited Cu/HEA C/CNLs

High-angle XRD spectra for the as-deposited Cu/HEA NLs with h spanning from 5 to 100 nm are shown in Fig. 1a. The FCC Cu layers show a strong (111) texture and a quite weak (200) texture, while the BCC HEA layers show a strong (110) texture and weak (200) and (211) textures. Typical cross-sectional TEM (XTEM) images of the as-deposited Cu/HEA NLs with different h are presented in Fig. 1b–f. The XTEM images of Cu/HEA NLs with h = 5, 10 and 50 nm show clear modulation structure and CCIs without notable intermixing, as shown in Fig. 1(b), (c, d) and (e, f), respectively. One can see that no large voids exist in the as-deposited NLs, and the interface bonding is good. It seems that the Cu layers always sustain the crystalline nature, while the HEA layers show the transition from fully crystalline structure at large h>10 nm to amorphous-like structure at small h≤10 nm. Both the sizes of columnar grains in the Cu and HEA layers scale with h. The corresponding selected area diffraction patterns (SADPs) in Fig. 1c and e manifest the diffraction rings of Cu (111) and (200) and HEA (110) and (200), which is in accordance with the XRD results.

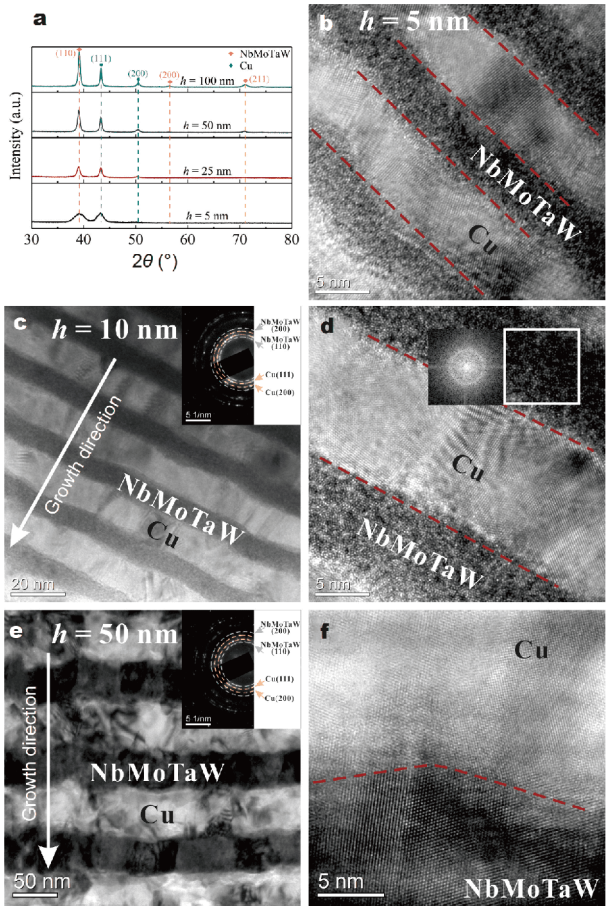

Figure 1 (a) XRD patterns for Cu/HEA NLs with different layer thicknesses h. Representative cross-sectional TEM images of Cu/HEA NLs with h = 10 (c) and 50 nm (e) showing clearly modulated structure. Typical HRTEM images of Cu/HEA NLs with h = 5 (b) and 10 nm (d) showing the amorphous-like microstructure of the HEA layers. (f) HRTEM images of Cu/HEA NLs with h = 50 nm. The corresponding SADPs inserted in (c, e) exhibit strong Cu (111) & (200) and HEA (110) & (200) textures.

Deformed microstructure of the indented Cu/HEA C/CNLs

Post-mortem TEM observations were carried out on representative Cu/HEA NLs with h = 50 nm indented at the strain rate of 0.1 s^{-1} to study the deformation behavior of constituents, as shown in Fig. 2. It appears that a shear band emerges in the Cu/HEA NLs associated with disruption of the hard HEA layers across the shear band (see Fig. 2a). Note that although such localized shearing deformation has been verified in h = 5 nm Cu/Nb NLs with an interfacial misfit strain of ~11.8% [36] and h = 12 nm

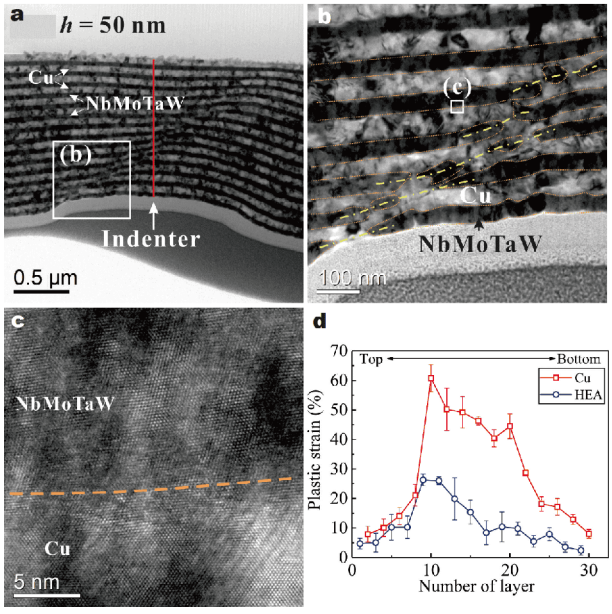

Figure 2 (a) The typical XTEM image of the indented Cu/HEA NLs with h = 50 nm, showing a shear band. (b) The magnified view of the boxed region in (a), showing fracture appears in the hard NbMoTaW layers of the highly deformed regions. (c) The HRTEM image of the boxed region in (b). (d) The plastic strain as a function of the number of layers for each constituent layer along the red solid line in (a), showing Cu layers dominate the plastic deformation.

© Science China Press and Springer-Verlag GmbH Germany, part of Springer Nature 2019

Cu/Cr NLs with the interfacial misfit strain of ~2.3% [37], the hard constituent layers are still intact after deformation at room temperature. Since the hardness of HEA (H ~12.6 GPa) is much higher than that of Cu (H ~1.7 GPa), the soft Cu layers dominate the plastic deformation and fracture firstly occurs in the hard HEA layers (see Fig. 2b). The plastic strain estimated from the difference of h before and after deformation for each constituent layer along the red solid line in Fig. 2a is displayed in Fig. 2d, exhibiting a Cu layer-dominated deformation. We further define a parameter $\xi = \sum_{i=1}^{n} \frac{\Delta h}{h}$ to evaluate the contributions from the constituents of Cu/HEA NLs to the total plastic deformation. It is found that the values of ξ for Cu and HEA layers in the Cu/HEA NLs are 0.77 and 0.23, respectively, implying Cu contributes much more to the total plastic strain of Cu/HEA NLs.

Mechanical properties of the Cu/HEA NLs

The typical indentation load-depth curves of the Cu/HEA NLs with different h at the same strain rate of 0.05 s^{-1} are displayed in Fig. 3a. The indentation depth of the Cu/HEA NLs decreases with reducing h from 100 to 50 nm, and then remains nearly constant with further reducing h. Accordingly, the hardness H of the Cu/HEA NLs increases from ~5.1 to ~6.0 GPa with h reducing from 100 to 50 nm, followed by a hardness plateau of ~5.9 GPa, as shown in Fig. 3b. The measured hardness of the Cu/HEA NLs is much lower than the calculated hardness *via* the ROM (H_{ROM} ~7.2 GPa), as indicated in Fig. 3b. A comparison of hardness between the present Cu/HEA NLs and reported FCC/BCC NLs are summarized in Fig. 3c, associated with their corresponding H_{ROM}. These NLs exhibit increased H with reducing h, and even show the hardness plateau at very small h. For Cu/Nb [20], Cu/Cr [22], Cu/Mo [34] and Cu/W [38], their peak hardnesses are larger than their H_{ROM} except for the Cu/Ta [39] and the present Cu/HEA samples. Moreover, the present Cu/HEA NLs have the longest peak hardness plateau, namely, the peak hardness can be achieved at large h ~50 nm.

Fig. 4a presents the strain rate dependent hardness of Cu/HEA NLs, in which the slope represents SRS index m and is summarized in Fig. 4b. The m of Cu/HEA NLs increases from ~0.007 to ~0.024 as h reduces from 100 to 25 nm, similar to the case of Cu/Mo [34], while decreases to a negative value about −0.012 with further decreasing h to 5 nm.

DISCUSSION

Interface-dominated deformation morphologies

As mentioned earlier, for the FCC/BCC C/CNLs, such as Cu/HEA, Cu/Nb and Cu/Cr systems, shear banding always occurs during indentation deformation accompanied with the thinning of hard constituent layers [36,37]. These findings indicate that shear banding at the small scale is favorable for FCC/BCC C/CNLs with incoherent CCIs. A possible reason is that the interfacial misfit dislocations can hinder the incoming dislocations from directly transmitting across the CCI, thereby promoting the asymmetric dislocation slip and dislocation-interface interactions to release residual dislocation and accommodate interface shear deformation [40]. In other words, the continuous thinning of constituent layers within the indentation-induced shear bands can be realized by the large shear stress component along the interface, which can refresh the capability of interfaces to absorb gliding dislocations through unlocking the product of the dislocation-interface reaction [20,40].

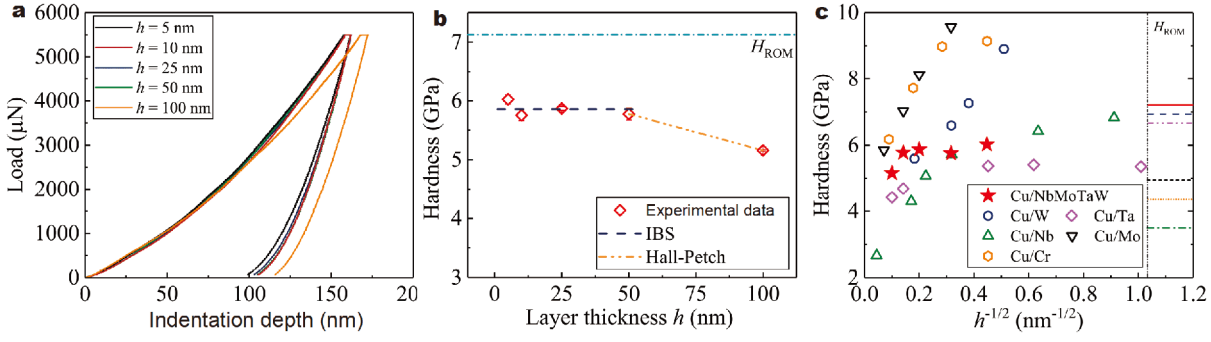

Figure 3 (a) Typical load-depth curves of Cu/HEA NLs with different h. The dependence of hardness H on the layer thickness h for (b) Cu/HEA NLs, compared with the hardness of NLs calculated from ROM. (c) The hardness H as a function of $h^{-1/2}$ for the present Cu/HEA NLs, compared with the reported FCC/BCC Cu/Nb [20], Cu/Cr [22], Cu/Mo [34], Cu/W [38] and Cu/Ta [39] NLs. The corresponding hardnesses H_{ROM} calculated from ROM are displayed at the right side in (c), as indicated by the lines with different colors.

 © Science China Press and Springer-Verlag GmbH Germany, part of Springer Nature 2019

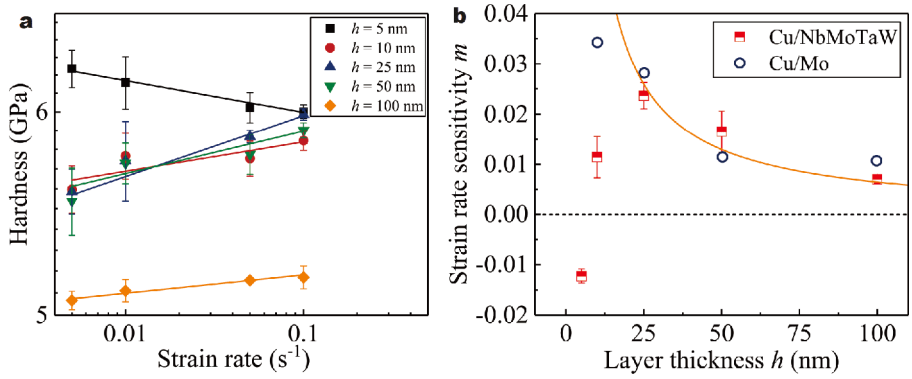

Figure 4 (a) Log hardness H *vs.* log strain rate plots of Cu/HEA NLs with different h, in which the slope of each line represents the SRS index m. (b) The m of Cu/HEA NLs as a function of h, compared with the reported Cu/Mo NLs [34], respectively. The lines in (b) are calculated by the present model. For details see the text.

Size-dependent hardness and strengthening mechanisms

To elucidate the size-dependent mechanical properties of the present Cu/HEA NLs, we first analyzed the deformation mechanisms of the soft constituent, i.e., Cu, since it yields first. Previous study has revealed that the deformation mechanism goes through a transition from partial to full dislocations nucleated from grain boundaries (GBs) in Cu at a critical size d_c, given by [42]

$$d_c = \frac{\eta}{\eta-1}\cdot\frac{\mu_{Cu}(3s-1)b_f^2}{3\gamma}, \quad (1)$$

where s ~2–4 is a stress factor, μ_{Cu} is the shear modulus, η is the ratio of grain size to equilibrium stacking fault width and $\eta/(\eta-1) \approx 1$, γ is the stacking fault energy (SFE), b_f is the magnitude of the Burgers vector of the full dislocations. Taking s = 3, μ_{Cu} = 48.3 GPa, $b_{f,Cu}$ = 0.2556 nm, γ_{Cu} = 41 mJ m^{-2}, the estimated critical size d_c is ~128.3 nm for Cu. This calculated critical size d_c is much larger than the characteristic size of Cu layers in the present Cu/HEA NLs, implying partial emission from boundaries is the dominated deformation mechanism. Therefore, based on the partial-based mechanism, in what follows we explain the size-dependent mechanical behavior of Cu/HEA NLs.

Previously, the size-dependent hardness of NLs with $h \geq$ 50 nm was widely captured by the Hall-Petch (H-P) model based on dislocations pile up against a CCI. Actually, prior studies [25,43,44] pointed out that the premise for dislocations pile-up in the soft constituent of NLs is that the applied shear stress (τ) less than one half of the IBS to slip transmission (τ_{int}) so that dislocations (with the number of $N > 2$) can pile up against the CCI in a slip plane, i.e., $N\cdot\tau \leq \tau_{int}$. For the present Cu/HEA NLs, the IBS τ_{int} can be theoretically estimated by [45,46]

$$\tau_{int} = \tau_d + \tau_k = \beta\mu_1^*\left(\zeta - \frac{b_f}{L}\right) + R\mu_1^*\frac{\sin\varphi}{8\pi}, \quad (2)$$

where the first term τ_d arises from misfit dislocation, β is Saada's constant, $\mu_1^* = 2\frac{\mu_{Cu}\cdot\mu_{HEA}}{\mu_{Cu}+\mu_{HEA}}$, is the mean shear modulus of the Cu/HEA NLs, ζ is the mismatch strain, L is the average spacing of the interface dislocation array; the second term τ_k is the Koehler stress, arising from the modulus mismatch, $R_1 = \frac{\mu_{HEA}-\mu_{Cu}}{\mu_{HEA}+\mu_{Cu}}$, φ is the angle between the slip plane and the CCI. Taking β = 0.41, μ_{HEA} = 108 GPa [47], $b_{f,HEA}$ = 0.28 nm, ζ = ~9%, φ = ~70.5°, L = ~2.75 nm, substituting Equation (2) into H = 2.7·M·τ = 8.37τ, the calculated IBS τ_{int} ~0.7 GPa or the peak hardness is ~5.86 GPa, which is in agreement with the experimental hardness plateau ~5.9 GPa (see Fig. 3b). This means that once the applied shear stress or the dislocation gliding stress reaches the IBS, individual dislocation in the soft phase can transmit across the CCI into the hard phase. Given the lowest hardness of the Cu/HEA NLs in the studied length scale is ~5.16 GPa at h = 100 nm, close to the hardness plateau, the dislocations pile-up in a slip plane with the number of dislocations $N \geq 2$ cannot form in the Cu layer. In this scenario, the traditional picture of dislocations pile-up determined by the IBS is questionable for the present Cu/HEA NLs.

In the present work, the hardness H of HEA film is very high ~12.6 GPa (much greater than the hardness plateau ~5.9 GPa), and the HEA layers exhibit local thinning, even rupture during deformation. This indicates that local stress concentrations must be induced, which contributes to the deformation of the hard HEA layers. In fact, although the interfacial barrier affects dislocation motion (e.g., confined slip in a layer and transmission

 © Science China Press and Springer-Verlag GmbH Germany, part of Springer Nature 2019

across a CCI), it does not disable the behavior of dislocations pile-up in laminated materials [48]. Compared with the coherent CCI with the unique slip continuity, the incoherent CCI renders the hard phase more difficulty in plastic deformation due to the discontinuity of slip systems between two constituents. However, the plastic deformation of the very hard phase is not determined by the interface structure with much lower IBS [48–50]. In other words, the strength of interfacial barrier can be overwhelmed by the stress concentration caused by the dislocations pile-up in the soft phase, which pushes the leading dislocation into the interface against the hard phase. Subsequently, the following dislocations move towards to the interface. When the stress concentration is high enough, the leading dislocation would trigger the plastic deformation of the hard phase. In such a case, the strength of the hard constituent rather than the interface determines whether the dislocations pile up. Thus, in the Cu/HEA NLs with low IBS, it is possible that dislocations are emitted from boundaries in Cu first and pile up eventually to realize the plastic deformation of the hard HEA layers. Specifically, when dislocations generate from GB ledges, the flow stress of pure metals follow the H-P (like) relationship according to the derivation by Li *et al.* [51] based on the theory of Taylor hardening. This rationalizes why the hardness of the Cu/HEA NLs with $h \geq$ 50 nm can be captured by the H-P (like) relationship, as indicated by the orange line in Fig. 3b.

Size-dependent strain rate sensitivity of Cu/HEA NLs

Prior results have uncovered that the size-dependent of m is closely related to the lattice structure of materials [22]. The m of FCC metals generally increases with reducing the grain size d from the micron-scale to the nano-scale. By contrast, BCC metals exhibit a reduced m [32] with reducing the grain size d to a critical size of ~50 nm, below which their m increases with further reducing d [52]. Overall, both FCC and BCC metals exhibit the positive m, i.e., faster strain rate leads to higher hardness. The rate dependence of the flow stress is normally attributed to the thermally activated process of overcoming the obstacles to dislocation motion. The m related to the activation volume V^* of the thermally activated event can be given by [53,54]

$$m = \frac{\sqrt{3}k_{\mathrm{B}}T}{\sigma V^*} = \frac{\sqrt{3}k_{\mathrm{B}}T}{\sigma b_p \chi l^*}, \tag{3}$$

where k_B is the Boltzman constant ~1.38×10^{-23} J K^{-1}, T is temperature ~298 K, χ is the distance (of the order of b_p) swept out by the mobile dislocation during an activation event and l^* is the effective dislocation segment. Assume the evolution of l^* is controlled by the geometrical length of microstructure L^*, one gets $l^* = \psi \cdot L^*$, where ψ is a proportionality factor. Based on the above theory, we discuss the underlying mechanisms of the size-dependent SRS for the Cu/HEA NLs as follows.

Given both Cu and HEA layers deform in the Cu/HEA NLs, following the derivation by Fan *et al.* [55], which involves the interface effect on the rate-limiting process, the m can be expressed as:

$$m = \xi_{\mathrm{Cu}} \cdot m_{\mathrm{Cu}} + \xi_{\mathrm{HEA}} \cdot m_{\mathrm{HEA}}, \tag{4}$$

where m_{Cu} and m_{HEA} are the SRS of Cu and HEA layers, respectively; ξ_{Cu} and ξ_{HEA} are the contributions of Cu and HEA layers to the total plastic strains, respectively. Since the flow stress has contributions from dislocations and GBs, both of which approximately follow the H-P-like strengthening behavior, the strength of constituents can be expressed as $\tau = \Lambda\sqrt{\rho} + \frac{\Omega}{\sqrt{h}}$ [56]. Thus, the m can be rewritten as:

$$m = \frac{k_{\mathrm{B}}T}{b^2} \cdot \frac{1}{\delta\left(\Lambda\sqrt{\rho}h + \Omega\sqrt{h}\right)}, \tag{5}$$

where ρ is the dislocation density, Λ, Ω and δ are retained as proportionality factors, other symbols have the same meaning as mentioned above. Taking $\rho = 5\times10^{12}$ cm^{-2}, δ = 30, Λ = 3.7 and Ω = 2, the calculation result agrees well with the experimental data when $h \geq$ 25 nm but much overestimates their m when $h <$ 25 nm, as indicated by the orange solid line in Fig. 4b. As $h \geq$ 25 nm, the HEA layers with d less than ~50 nm manifest increased m with reducing the layer or grain size [35], similar to that of FCC Cu. Therefore, the m of NLs increases with decreasing h, as supported by the findings in Cu/Mo [34]. As $h <$ 25 nm, the m of NLs is reduced, even becomes negative at small h = 5 nm. This can be related to the amorphous-like microstructure of the NbMoTaW layers often with negative m [30,57], which behave oppositely to the FCC Cu. Hence, the competing effect between Cu and NbMoTaW renders a maximum m at h = 25 nm.

CONCLUSION

In this work, we reveal the size-dependent deformation behavior of Cu/HEA (HEA = NbMoTaW) NLs. The interfacial structure significantly affects the plastic deformation behavior resulting in the shear banding in the Cu/HEA system. The dislocations pile-up in soft Cu layers that dominates the plastic deformation of the Cu/HEA NLs with large h is determined by the maximum

 © Science China Press and Springer-Verlag GmbH Germany, part of Springer Nature 2019

strength value between the hard HEA and the interfacial barrier. The Cu/HEA NLs exhibit a maximum m at a critical h, which is caused by the transition from the synergetic effect of crystalline constituents above the critical size to the competitive effect between the crystalline Cu and amorphous-like HEA below the critical size. These main findings provide new insights into designing the nanolaminated materials containing HEAs with desirable mechanical properties.

Received 31 July 2019; accepted 23 September 2019; published online 7 November 2019

1 Yeh JW, Chen SK, Lin SJ, *et al.* Nanostructured high-entropy alloys with multiple principal elements: Novel alloy design concepts and outcomes. Adv Eng Mater, 2004, 6: 299–303
2 Cantor B, Chang ITH, Knight P, *et al.* Microstructural development in equiatomic multicomponent alloys. Mater Sci Eng-A, 2004, 375-377: 213–218
3 Zhang Y, Zuo TT, Tang Z, *et al.* Microstructures and properties of high-entropy alloys. Prog Mater Sci, 2014, 61: 1–93
4 Zhang W, Liaw PK, Zhang Y. Science and technology in high-entropy alloys. Sci China Mater, 2018, 61: 2–22
5 Ganji RS, Sai Karthik P, Bhanu Sankara Rao K, *et al.* Strengthening mechanisms in equiatomic ultrafine grained AlCoCrCuFeNi high-entropy alloy studied by micro- and nanoindentation methods. Acta Mater, 2017, 125: 58–68
6 Zou Y, Ma H, Spolenak R. Ultrastrong ductile and stable high-entropy alloys at small scales. Nat Commun, 2015, 6: 7748
7 He JY, Liu WH, Wang H, *et al.* Effects of al addition on structural evolution and tensile properties of the FeCoNiCrMn high-entropy alloy system. Acta Mater, 2014, 62: 105–113
8 Li D, Li C, Feng T, *et al.* High-entropy $Al_{0.3}$CoCrFeNi alloy fibers with high tensile strength and ductility at ambient and cryogenic temperatures. Acta Mater, 2017, 123: 285–294
9 Liu J, Guo X, Lin Q, *et al.* Excellent ductility and serration feature of metastable cocrfeni high-entropy alloy at extremely low temperatures. Sci China Mater, 2019, 62: 853–863
10 Juan CC, Tsai MH, Tsai CW, *et al.* Enhanced mechanical properties of HfMoTaTiZr and HfMoNbTaTiZr refractory high-entropy alloys. Intermetallics, 2015, 62: 76–83
11 Tsai MH, Yeh JW, Gan JY. Diffusion barrier properties of AlMoNbSiTaTiVZr high-entropy alloy layer between copper and silicon. Thin Solid Films, 2008, 516: 5527–5530
12 Tang Z, Yuan T, Tsai CW, *et al.* Fatigue behavior of a wrought $Al_{0.5}$CoCrCuFeNi two-phase high-entropy alloy. Acta Mater, 2015, 99: 247–258
13 Gludovatz B, Hohenwarter A, Catoor D, *et al.* A fracture-resistant high-entropy alloy for cryogenic applications. Science, 2014, 345: 1153–1158
14 Maiti S, Steurer W. Structural-disorder and its effect on mechanical properties in single-phase TaNbHfZr high-entropy alloy. Acta Mater, 2016, 106: 87–97
15 Schuh B, Mendez-Martin F, Völker B, *et al.* Mechanical properties, microstructure and thermal stability of a nanocrystalline CoCrFeMnNi high-entropy alloy after severe plastic deformation. Acta Mater, 2015, 96: 258–268
16 Fu Z, Chen W, Wen H, *et al.* Microstructure and strengthening mechanisms in an fcc structured single-phase nanocrystalline $Co_{25}Ni_{25}Fe_{25}Al_{7.5}Cu_{17.5}$ high-entropy alloy. Acta Mater, 2016, 107: 59–71
17 Fan JT, Zhang LJ, Yu PF, *et al.* A novel high-entropy alloy with a dendrite-composite microstructure and remarkable compression performance. Scripta Mater, 2019, 159: 18–23
18 Lu K, Lu L, Suresh S. Strengthening materials by engineering coherent internal boundaries at the nanoscale. Science, 2009, 324: 349–352
19 Ritchie RO. The conflicts between strength and toughness. Nat Mater, 2011, 10: 817–822
20 Misra A, Verdier M, Lu YC, *et al.* Structure and mechanical properties of Cu-X (X = Nb, Cr, Ni) nanolayered composites. Scripta Mater, 1998, 39: 555–560
21 Yan JW, Zhu XF, Yang B, *et al.* Shear stress-driven refreshing capability of plastic deformation in nanolayered metals. Phys Rev Lett, 2013, 110: 155502
22 Niu JJ, Zhang JY, Liu G, *et al.* Size-dependent deformation mechanisms and strain-rate sensitivity in nanostructured Cu/X (X=Cr, Zr) multilayer films. Acta Mater, 2012, 60: 3677–3689
23 Beyerlein IJ, Wang J. Interface-driven mechanisms in cubic/non-cubic nanolaminates at different scales. MRS Bull, 2019, 44: 31–39
24 Beyerlein IJ, Demkowicz MJ, Misra A, *et al.* Defect-interface interactions. Prog Mater Sci, 2015, 74: 125–210
25 Liu Y, Bufford D, Wang H, *et al.* Mechanical properties of highly textured Cu/Ni multilayers. Acta Mater, 2011, 59: 1924–1933
26 Zhang JY, Wu K, Zhang LY, *et al.* Unraveling the correlation between Hall-Petch slope and peak hardness in metallic nanolaminates. Int J Plast, 2017, 96: 120–134
27 Knorr I, Cordero NM, Lilleodden ET, *et al.* Mechanical behavior of nanoscale Cu/PdSi multilayers. Acta Mater, 2013, 61: 4984–4995
28 Fan Z, Xue S, Wang J, *et al.* Unusual size dependent strengthening mechanisms of Cu/amorphous CuNb multilayers. Acta Mater, 2016, 120: 327–336
29 Liu Y, Yang KM, Hay J, *et al.* The effect of coherent interface on strain-rate sensitivity of highly textured Cu/Ni and Cu/V multilayers. Scripta Mater, 2019, 162: 33–37
30 Wang YQ, Zhang JY, Liang XQ, *et al.* Size- and constituent-dependent deformation mechanisms and strain rate sensitivity in nanolaminated crystalline Cu/amorphous Cu-Zr films. Acta Mater, 2015, 95: 132–144
31 Chen J, Lu L, Lu K. Hardness and strain rate sensitivity of nanocrystalline cu. Scripta Mater, 2006, 54: 1913–1918
32 Wei Q, Ramesh KT, Ma E, *et al.* Plastic flow localization in bulk tungsten with ultrafine microstructure. Appl Phys Lett, 2005, 86: 101907
33 Karimpoor A. High strength nanocrystalline cobalt with high tensile ductility. Scripta Mater, 2003, 49: 651–656
34 Zhang JY, Zeng FL, Wu K, *et al.* Size-dependent plastic deformation characteristics in He-irradiated nanostructured Cu/Mo multilayers: Competition between dislocation-boundary and dislocation-bubble interactions. Mater Sci Eng-A, 2016, 673: 530–540
35 Feng XB, Zhang JY, Wang YQ, *et al.* Size effects on the mechanical properties of nanocrystalline NbMoTaW refractory high entropy alloy thin films. Int J Plast, 2017, 95: 264–277
36 Bhattacharyya D, Mara NA, Dickerson P, *et al.* Transmission electron microscopy study of the deformation behavior of Cu/Nb and Cu/Ni nanoscale multilayers during nanoindentation. J Mater Res, 2011, 24: 1291–1302
37 Li YP, Zhu XF, Tan J, *et al.* Comparative investigation of strength

 © Science China Press and Springer-Verlag GmbH Germany, part of Springer Nature 2019

and plastic instability in Cu/Au and Cu/Cr multilayers by indentation. J Mater Res, 2009, 24: 728–735
38 Wen S, Zong R, Zeng F, *et al.* Evaluating modulus and hardness enhancement in evaporated Cu/W multilayers. Acta Mater, 2007, 55: 345–351
39 Wei MZ, Cao ZH, Shi J, *et al.* Anomalous plastic deformation in nanoscale Cu/Ta multilayers. Mater Sci Eng-A, 2014, 598: 355–359
40 Zeng Y, Hunter A, Beyerlein IJ, *et al.* A phase field dislocation dynamics model for a bicrystal interface system: An investigation into dislocation slip transmission across cube-on-cube interfaces. Int J Plast, 2016, 79: 293–313
41 Subedi S, Beyerlein IJ, LeSar R, *et al.* Strength of nanoscale metallic multilayers. Scripta Mater, 2018, 145: 132–136
42 Asaro RJ, Suresh S. Mechanistic models for the activation volume and rate sensitivity in metals with nanocrystalline grains and nanoscale twins. Acta Mater, 2005, 53: 3369–3382
43 Misra A, Hirth JP, Hoagland RG. Length-scale-dependent deformation mechanisms in incoherent metallic multilayered composites. Acta Mater, 2005, 53: 4817–4824
44 Chen Y, Liu Y, Sun C, *et al.* Microstructure and strengthening mechanisms in Cu/Fe multilayers. Acta Mater, 2012, 60: 6312–6321
45 Rao SI, Hazzledine PM. Atomistic simulations of dislocation-interface interactions in the Cu-Ni multilayer system. Philos Mag A, 2000, 80: 2011–2040
46 Koehler JS. Attempt to design a strong solid. Phys Rev B, 1970, 2: 547–551
47 Zou Y, Maiti S, Steurer W, *et al.* Size-dependent plasticity in an $Nb_{25}Mo_{25}Ta_{25}W_{25}$ refractory high-entropy alloy. Acta Mater, 2014, 65: 85–97
48 Zhang X, Godfrey A, Huang X, *et al.* Microstructure and strengthening mechanisms in cold-drawn pearlitic steel wire. Acta Mater, 2011, 59: 3422–3430
49 Kapp MW, Hohenwarter A, Wurster S, *et al.* Anisotropic deformation characteristics of an ultrafine- and nanolamellar pearlitic steel. Acta Mater, 2016, 106: 239–248
50 Chen W, Zhang J, Cao S, *et al.* Strong deformation anisotropies of ω-precipitates and strengthening mechanisms in Ti-10V-2Fe-3Al alloy micropillars: Precipitates shearing vs precipitates disordering. Acta Mater, 2016, 117: 68–80
51 Li JCM, Chou YT. The role of dislocations in the flow stress grain size relationships. Metall Materi Trans, 1970, 1: 1145–1159
52 Malow TR, Koch CC, Miraglia PQ, et al. Compressive mechanical behavior of nanocrystalline Fe investigated with an automated ball indentation technique. Mater Sci Eng: A, 1998, 252: 36–43
53 Cheng S, Ma E, Wang Y, *et al.* Tensile properties of *in situ* consolidated nanocrystalline Cu. Acta Mater, 2005, 53: 1521–1533
54 Bouaziz O. Strain-hardening of twinning-induced plasticity steels. Scripta Mater, 2012, 66: 982–985
55 Fan Z, Liu Y, Xue S, *et al.* Layer thickness dependent strain rate sensitivity of Cu/amorphous CuNb multilayer. Appl Phys Lett, 2017, 110: 161905
56 Wei Q, Cheng S, Ramesh KT, *et al.* Effect of nanocrystalline and ultrafine grain sizes on the strain rate sensitivity and activation volume: fcc *versus* bcc metals. Mater Sci Eng-A, 2004, 381: 71–79
57 Dalla Torre FH, Dubach A, Siegrist ME, *et al.* Negative strain rate sensitivity in bulk metallic glass and its similarities with the dynamic strain aging effect during deformation. Appl Phys Lett, 2006, 89: 091918

Acknowledgements This work was supported by the National Natural Science Foundation of China (51621063, 51722104, 51625103, 51790482, 51761135031 and 51571157), the National Key Research and Development Program of China (2017YFA0700701 and 2017YFB0702301), the 111 Project 2.0 of China (BP2018008), the International Joint Laboratory for Micro/Nano Manufacturing and Measurement Technologies, and the Fundamental Research Funds for the Central Universities (xzy022019071). Zhang J is grateful for the Fok Ying-Tong Education Foundation (161096), China Postdoctoral Science Foundation (2017T100744) and Shaanxi Province innovative talents promotion Projects (2018KJXX-004). Wu K thanks the support from China Postdoctoral Science Foundation (2016M602811). We thank Dr. Guo SW of Xi'an Jiaotong University (XJTU) and Dr. Li J at the Instrument Analysis Center of XJTU for their great assistance in TEM analysis.

Author contributions Sun J and Liu G supervised the project. Zhang J initiated the research concept. Zhao Y, Wang Y and Wu K conducted the experiments. Zhang J, Liu G and Sun J interpreted the results and wrote the manuscript, with significant input from all other authors.

Conflict of interest The authors declare that they have no conflict of interest.

Yufang Zhao received her BSc from the Xi'an Jiaotong University in 2016 and is now a PhD candidate under the supervision of Prof. Jun Sun at the College of Material Science and Engineering in Xi'an Jiaotong University. Her current research interest is the mechanical behavior of nanolaminates.

Jinyu Zhang earned his BSc degree from Lanzhou University of Technology (2005), and PhD degree (2011) in material science and engineering from Xi'an Jiaotong University. He joined Prof. Liu Gang's group in 2012 and was promoted to professor in 2017. His research focuses on the strengthening & toughening and deformation of nanostructured metals.

Gang Liu obtained his BSc degree from Wuhan University of Science and Technology (1996) and PhD degree in material science and engineering from Xi'an Jiaotong University in 2002. In 2005, he joined Prof. Jun Sun's group as an associate professor and was promoted to professor in 2008. His current research focuses on the aging dynamics of aluminum alloy and its simulation, and quantitative relationship between microstructure and macroscopic properties of materials.

 © Science China Press and Springer-Verlag GmbH Germany, part of Springer Nature 2019

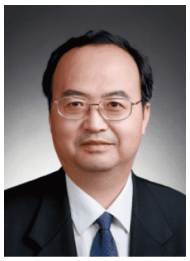

Jun Sun obtained his BSc degree from Jilin University (1982) and PhD degree in material science and engineering from Xi'an Jiaotong University in 1989. In 2002, he joined the State Key Laboratory for Mechanical Behavior of Materials in Xi'an Jiaotong University, where he is currently professor and group leader. His research focuses on the multiscale effect of materials' deformation and transformation, and microstructure optimization and mechanical properties enhancement of metals.

Cu/NbMoTaW纳米叠层材料具有尺寸效应的力学性能及变形机制

赵宇芳, 张金钰*, 王亚强, 吴凯, 刘刚*, 孙军*

摘要 高熵合金(HEA)由于其在恶劣环境中优异的力学性能引起了研究者的广泛关注. 我们将高熵合金NbMoTaW引入到纳米叠层材料中, 制备出等层厚的Cu/HEA纳米多层膜, 综合研究了其具有尺寸效应的力学性能及变形行为. 实验表明, Cu/HEA纳米多层膜的硬度随着层厚h的减小而增加, 随后在$h\leq$50 nm的区域到达一个平台, 而应变速率敏感性出现了一个最大值, 这是由于Cu和HEA两相对应变速率敏感性的影响从协同转变为竞争. 在层厚较大时, 非共格界面导致Cu/HEA多层膜在变形后出现了剪切带, 并且软相Cu层主导变形.

© Science China Press and Springer-Verlag GmbH Germany, part of Springer Nature 2019